Chapter

Analysis of Energy Relations between Noise and Vibration Produced by a Low-Field MRI Device

Jiří Přibil, Anna Přibilová and Ivan Frollo

Abstract

Magnetic resonance imaging (MRI) tomography is often used for noninvasive scanning of various parts of a human body without undesirable effects present in X-ray computed tomography. In MRI devices, slices of a tested subject are selected in 3D coordinates by a system of gradient coils. The current flowing through these coils changes rapidly, which results in mechanical vibration. This vibration is significant also in the equipment working with a low magnetic field, and it causes image blurring of thin layer samples and acoustic noise significantly degrading a speech signal recorded simultaneously during MR scanning of the vocal tract. There are always negative physiological and psychological effects on a person exposed to vibration and acoustic noise. In order to minimize these negative impacts depending on intensity and time duration of exposition, we mapped relationship between energy of vibration and noise signals measured in the MRI scanning area and its vicinity.

Keywords: magnetic resonance imaging, acoustic noise, mechanical vibration, statistical analysis, low magnetic field environment

1. Introduction

The magnetic resonance imaging (MRI) method is successfully used for monitoring progress in therapy after vocal fold cancer surgery or for monitoring of the implanted cartilage in legs or arms, and/or the process of regeneration in different tissues, etc. In the case of the open-air MRI device, a weak magnetic field (up to 0.2 T) is usually generated by a pair of permanent magnets. Between these magnets, the gradient system consisting of 2×3 planar coils is situated together with the RF receiving/transmitting coils surrounding the tested object [1]. Slices of a tested object are selected in 3D coordinates by a gradient system consisting of planar coils parallel to the magnets. A rapidly changing current flowing through the gradient coils produces significant mechanical vibration [2, 3] causing blurring of images of thin layer samples and acoustic noise significantly degrading the speech signal recorded simultaneously during MR scanning of the human vocal tract [4, 5]. Acoustic noise has always negative physiological and psychological consequences on the exposed person depending on the noise intensity and time duration of noise

exposure [6]. In order to minimize these negative factors, this work is focused on mapping of energy relationship between vibration and noise signals measured in the MRI scanning area and its vicinity with the final aim to choose the proper scan sequence and its parameters—repetition time (TR), echo time (TE), orientation of scan slices, etc. Apart from real-time recording of the vibration and noise signals, the sound pressure level (SPL) was measured by a sound level meter using frequency weighting to match human perception of noise. The measured data and recorded signals were further processed off-line—the determined energetic features were statistically analyzed and the results were compared visually and numerically.

2. Subject and methods

As mentioned above, the open-air MRI device is primarily used in medical diagnostics, so designation of three planes formed by x, y, and z axes follows medical terminology used for human body planes [7]. The plane dividing the body vertically into ventral (anterior) and dorsal (posterior) parts is called a coronal (frontal) plane. The second vertical plane dividing the body to left and right sides is a sagittal plane. The horizontal plane that divides the human body into superior (upper) and inferior (lower) parts is called a transverse (cross-sectional) plane. During sequence execution, the gradient coil pair corresponding to the chosen scan orientation is activated, it consequently vibrates, and acoustic noise is radiated in the surrounding air. Two basic types of sequences called spin echo (SE) and gradient echo (GE) arising from MRI physical principles [8] are preferred in this type of MRI device. The volume size of the tested object/subject is another important factor having an influence on the intensity of the produced vibration and noise in the scanning area of the MRI device. A tested person/sample/phantom as a part of the whole vibrating mechanical system changes the overall mass, stiffness, and damping by loading the lower gradient coil structure in the patient's bed.

2.1 Sensors for measurement in a weak magnetic field environment

If the vibration and noise signals are recorded during MR scanning, interaction with the stationary magnetic field B_0 in the scanning area must be eliminated; otherwise, the quality of the acquired images would not be preserved. It means that the vibration sensors placed in the MRI scanning area with the static magnetic field cannot contain any part made from a ferromagnetic material. In MRI equipment, working with a weak magnetic field the interaction problem can be solved by a proper choice of the measuring device and its arrangement. Usually, it is sufficient to locate it in an adequate distance from the noise signal source outside the magnetic field area. Since the noise intensity as well as its spectral properties depends on the position of the measuring instrument, the recording/measuring microphone must have high sensitivity, an appropriate pickup pattern, type of the microphone, and a position in regard to the central point of the MRI scanning area (distance, direction angle, working height). The best solution is to use a microphone with a variable pattern having two diaphragms that share a common back plate. Such a microphone behaves as two back-to-back cardioid microphones. If one membrane is connected to a constant polarization voltage and the second one is polarized by a variable voltage, principally any directional pattern can be created. Basic omnidirectional, figure-of-eight, and cardioid patterns corresponding to both same voltages of the same polarity, the opposite polarity, and one zero voltage are represented in an ideal form by a polar equation:

$$\rho(\theta) = A + B \cdot \cos\theta, \qquad A + B = 1, \tag{1}$$

where $A = 1$, $B = 0$ for omnidirectional, $A = 0$, $B = 1$ for figure-of-eight, and $A = 0.5$, $B = 0.5$ for cardioid directional patterns.

The noise distribution in the scanning area of the MRI equipment and its neighborhood has to be mapped prior to the selection of the proper recording microphone location. C-weighting was used for SPL measurement to accommodate the objective noise intensity to the subjective loudness at high sound levels. The C-weighting filter frequency response in s-domain is given by the equation

$$H(s) = G \cdot \frac{\left(2\pi f_2\right)^2 \cdot s^4}{\left(s + 2\pi f_1\right)^2 \cdot \left(s + 2\pi f_2\right)^2}, \tag{2}$$

where $f_1 = 20.6$ Hz, $f_2 = 12{,}194$ Hz, and $20 \log G = 0.062$ dB [9]. To get the transfer function of the digital IIR filter, the frequency scale is warped by the bilinear transform from s-plane to z-plane

$$s \rightarrow 2 \cdot \frac{1 - z^{-1}}{1 + z^{-1}}. \tag{3}$$

The sensors measuring vibration signals are placed inside the MRI scanning area where the basic stationary magnetic field of the MRI device is present together with the superimposed pulse magnetic field generated by the gradient system as well as the high voltage field originated during activation of the excitation RF coil. These fields would disturb a signal picked up by the sensor from ferromagnetic material or damage electronics integrated with the sensor [10, 11], which can be avoided using the vibration sensor with a piezoelectric transducer. The sensor must have good sensitivity and maximally flat frequency response with the frequency range covering the vibration and noise harmonic frequencies that fall into the low band due to frequency-limited gradient pulses. As a similar frequency range can be found in basic processing of speech signals, it is very important in the case of 3D scanning of the human vocal tract by MRI with parallel recording of a speech signal [5].

The mentioned requirements imposed on the vibration sensor can be met by the sensor for acoustic musical instruments [12]. Its first usage in the magnetic field environment must be preceded by a calibration procedure and a measurement of its sensitivity and frequency response. The measured frequency response is used to determine a correction curve for filtering of the picked-up vibration signal and consecutive linearization operation that has effect on correctness of all analyzed spectral properties determined from the vibration signals—see the block diagram in **Figure 1**. The correction filter is proposed by a standard procedure of second-order shelving filter design [13]:

$$H(z) = \frac{b_0 + b_1 z^{-1} + b_2 z^{-2}}{a_0 + a_1 z^{-1} + a_2 z^{-2}}. \tag{4}$$

For the sampling frequency f_s, the polynomial filter coefficients $a_{0,1,2}$ and $b_{0,1,2}$ are derived from three input parameters—gain G, mid-point frequency f_c, and quality factor Q—in the following manner:

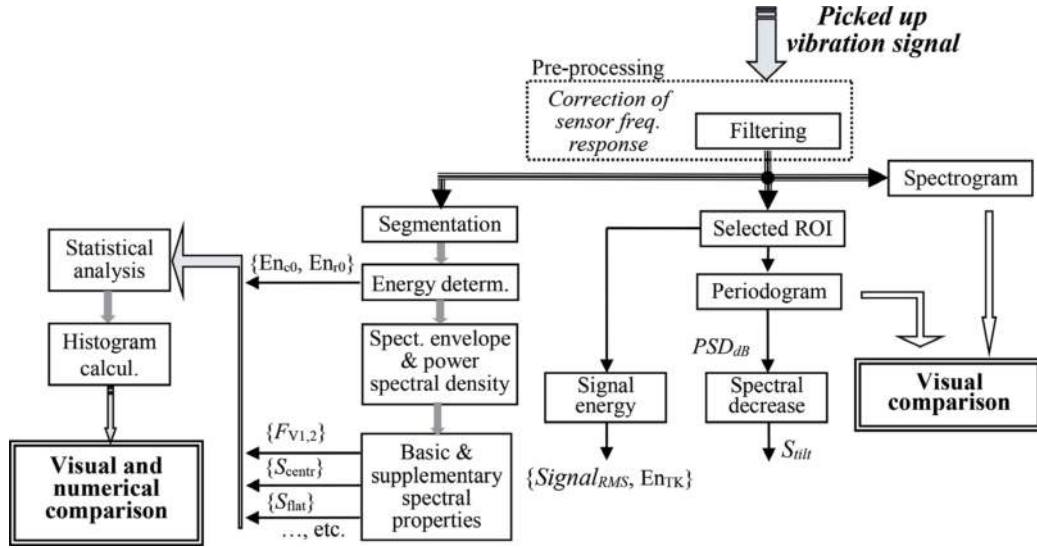$$A = 10^{\frac{G}{20}}, \; \omega_c = 2\pi \cdot \frac{f_c}{f_s}, \tag{5}$$

Figure 1.
Block diagram of processing of the picked-up vibration signal.

$$q_s = \frac{\sqrt{A}}{Q} \cdot \sin \omega_c, \quad q_{c1} = (A+1) \cdot \cos \omega_c, \quad q_{c2} = (A-1) \cdot \cos \omega_c, \tag{6}$$

$$a_0 = A + 1 - q_{c2} + q_s, \quad a_1 = 2 \cdot [A - 1 - q_{c1}], \quad a_2 = a_0 - 2q_s, \tag{7}$$

$$b_0 = A \cdot [A + 1 + q_{c2} + q_s], \quad b_1 = -2A \cdot [A - 1 + q_{c1}], \quad b_2 = b_0 - 2q_s. \tag{8}$$

2.2 Features for description of vibration and noise signals

Several methods can be used to determine the energy of a periodical signal:

- The standard root mean square (RMS) is calculated from a signal $x(n)$ in a defined region of interest (ROI) with the length of M samples

$$Signal_{RMS} = \sqrt{\frac{1}{M} \sum_{n=1}^{M} |x(n)|^2}. \tag{9}$$

- The absolute value of the mean of the Teager-Kaiser energy operator O_{TK} [14] is used to calculate the energy En_{TK}

$$O_{TK} = x(n)^2 - x(n-1) \cdot x(n+1), \quad En_{TK} = abs\left(\frac{1}{M-2} \sum_{n=1}^{M-2} O_{TK}(n)\right). \tag{10}$$

- The frame energy is estimated by the first cepstral coefficient c_0 or the autocorrelation coefficient r_0 after processing the signal $x(n)$ in frames using N_{FFT}-point FFT to compute magnitude spectrum and power spectrum $|S(k)|^2$,

$$En_{c0} = \sqrt{\left[\prod_{k=1}^{N_{FFT}/2} |S(k)|^2\right]^{\frac{2}{N_{FFT}}}}, \quad En_{r0} = \frac{2}{N_{FFT}} \sum_{k=1}^{N_{FFT}/2} |S(k)|^2. \tag{11}$$

For basic visual comparison of spectral properties of the recorded vibration and noise signals, the periodogram representing an estimate of the power spectral density (PSD) can be successfully used. The basic spectral properties can be determined from the spectral envelope, and subsequently, the histograms of spectral values can be calculated and compared. They also include the basic resonance frequencies F_{V1} and F_{V2} and their ratios, and the spectral decrease (tilt-S_{tilt}) as the degree of fall of the power spectrum calculated by a linear regression using the mean square method.

The supplementary spectral features describe the shape of the power spectrum of the noise signal. The spectral centroid (S_{centr}) determines a center of gravity of the spectrum—the average frequency weighted by the values of the normalized energy of each frequency component in the spectrum

$$S_{centr} = \frac{f_s}{N_{FFT}} \cdot \frac{\sum_{k=1}^{N_{FFT}} k|S(k)|^2}{\sum_{k=1}^{N_{FFT}} |S(k)|^2}.$$ (12)

The spectral flatness (S_{flat}) is useful to determine the degree of periodicity in the signal, and it can be calculated as a ratio of the geometric and the arithmetic mean values of the power spectrum

$$S_{flat} = \frac{\left[\prod_{k=1}^{N_{FFT}} |S(k)|^2 \right]^{\frac{2}{N_{FFT}}}}{\frac{2}{N_{FFT}} \sum_{k=1}^{N_{FFT}} |S(k)|^2}.$$ (13)

The spectral entropy is a measure of spectral distribution. It quantifies a degree of randomness of spectral probability density represented by normalized frequency components of the spectrum. The Shannon spectral entropy (SHE) can be calculated using the following formulas:

$$SHE = -\sum_{k=1}^{N_{FFT}} |S(k)|^2 \log_2 |S(k)|^2.$$ (14)

3. Description of performed measurements and experiments

The performed measurements were focused on analysis of vibration and noise conditions in the scanning area and in the neighborhood of the open-air MRI equipment E-scan Opera by Esaote S.p.A., Genoa [15] located at the Institute of Measurement Science, SAS, Bratislava. The experiments were realized in four steps: in the preliminary phase, the calibration was carried out, and the sensitivity and the frequency response of the used vibration sensor were determined. Next, the noise was measured using different directional patterns of the pickup microphone and the influence of the pickup pattern on the spectral properties of the recorded noise signal was analyzed. Then, the main vibration and noise measurement and recording experiment were realized. The recorded signals were subsequently processed and statistically analyzed. Finally, a detailed analysis of the influence of chosen scan parameters on the time duration of the used MR sequences and on the quality factor of the MR images was performed with the aim to find a suitable setting to minimize exposition of the examined persons to noise and vibration.

3.1 Calibration of vibration sensors suitable for measurement in the low magnetic field environment

The calibration and measurement experiments were realized with the help of the main devices: the Audio Precision System One including two programmable input and output channels for simultaneous measurement of electrical signals from the vibration sensors mounted on the Vibration Exciter ESE 201 located at the Institute of Electronics and Photonics, FEE&IT SUT, Bratislava. As a reference sensor, the accelerometer KD35a from the company Metra Mess- und Frequenztechnik was used. The sensor sensitivity of this standardized accelerometer is guaranteed, and it operates over a frequency range from 50 Hz to 10 kHz. Three types of vibration sensors having good response in the lower audio frequency range up to 2 kHz were tested within this work:

- Cejpek SB-1 with the thin circular brass disc of 0.25-mm thickness and 27.5-mm diameter designed primarily for pickup of a musical sound of a contrabass (further called as "*SB-1*"),

- Shadow SH-SB2 double bass pickup with two disc transducers of 0.5-mm thickness and 22.5-mm diameter (further called as "*SB2a,b*"),

- RFT heart microphone device HM 692 comprising a piezo-electric element integrated in the 1-mm thin aluminum metal cover with 30-mm diameter (further called as "*HM692*").

The sensors were mounted on the plate of the vibration exciter as shown in the detailed photo of the arrangement of the sensors in the right part of **Figure 2**. The output voltage for supply of this exciter and the signal from the calibrated sensors were checked parallel by the digital oscilloscope Rigol DS1102E. Two types of the parameters of the vibration sensors were measured and compared in our experiment:

- relative sensitivity at the reference frequency f_{ref} = 125 Hz,

- frequency response in the range from 20 Hz to 2 kHz at the chosen output voltage of the vibration exciter (U_{excBa0} = 360 mV).

Dependence of the sensor's sensitivity on the excitation voltage for all three sensors is presented in **Figure 3a**. The reference voltage sensitivity B_{a0} of the SB-1
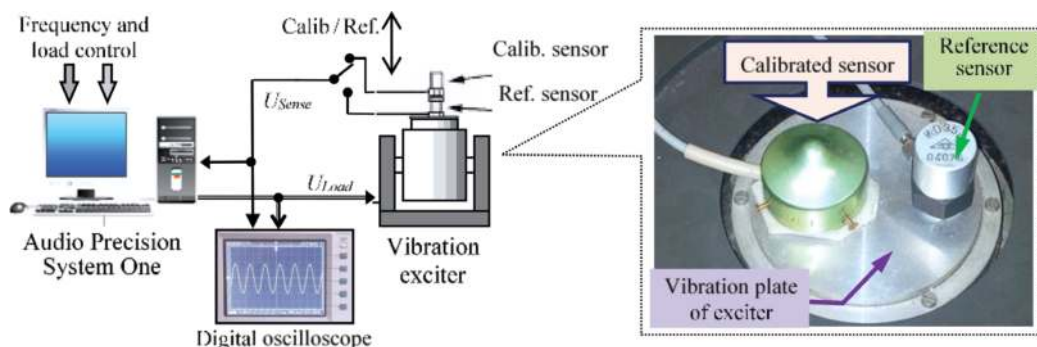

Figure 2.
Principle block diagram of the used calibration and measurement method together with a detailed photo of practical mounting of the sensors on the plate of the vibration exciter.
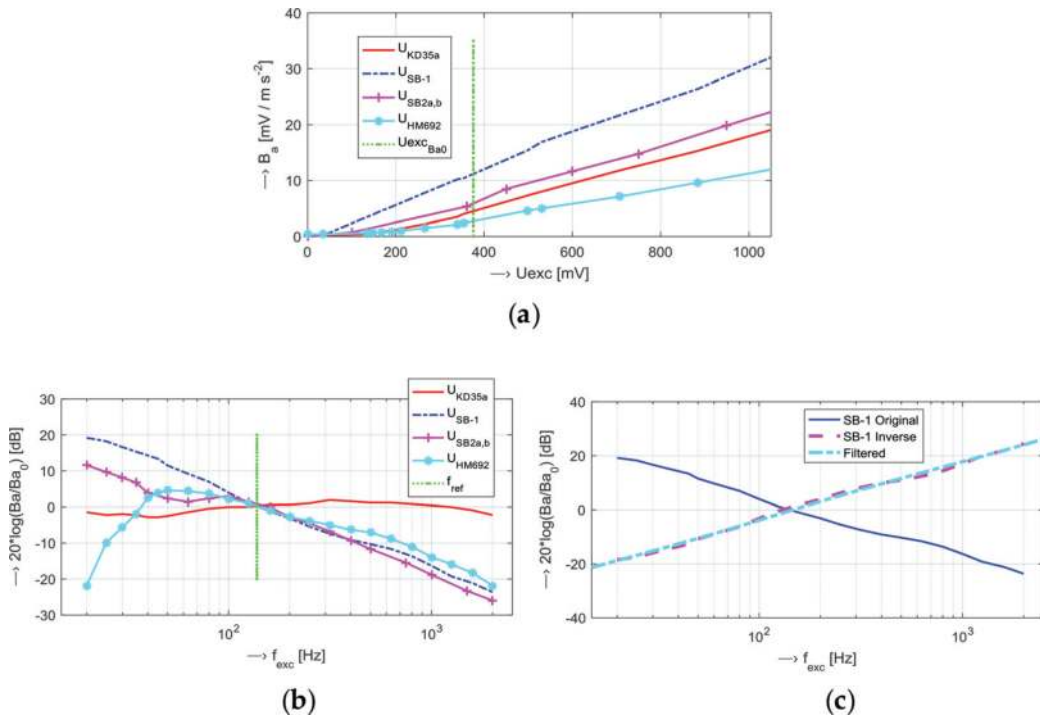
Figure 3.
Graph of: (a) measured sensors' sensitivities, (b) frequency responses in the range 20 Hz to 2 kHz measured and recalculated in [dB], and (c) correction frequency response for the SB-1 sensor linearization using the shelving filter (b): f_{ref} = 125 Hz, $Uexc_{Bao}$ = 360 mV, B_{ao} = {3.69 (KD35a), 12.9 (SB-1), 5.65 (SB2ab), and 2.45 (HM692)} mV/m s^{-2}.

sensor was determined from this graph. Comparison in **Figure 3b** shows that the measured frequency responses of SB-1, SB2ab, and HM692 are rotated by a slope of about −20 dB per decade with respect to the frequency response of KD35a. As the reference KD35a is an acceleration sensor, it emerges that the remaining three sensors are velocity ones. The calculated inverse frequency response of the SB-1 is drawn by the magenta dashed line together with the correction frequency response obtained by shelving equalization that is plotted by the cyan dot-dash line in **Figure 3c**. The effect of this shelving filter on the time-domain vibration signal, its frequency-domain periodogram with chosen spectral features, and the spectrogram can be seen in **Figure 4**.

3.2 Analysis of the influence of the directional pattern of the pickup microphone on the spectral properties of the recorded noise signal

Acoustic noise measurement in the MRI neighborhood was realized in the directions of 30, 90, and 150°, at the distance of 60 cm from the central point of the scanning area, and at the height of 85 cm from the floor—see the principal arrangement photo in **Figure 5**. In this noise recording part of the experiment, the pick-up Behringer dual-diaphragm condenser microphone B-2 PRO with switchable cardioid, omnidirectional, or figure-of-eight pickup patterns was used—see the directional patterns from the manufacturer's specification sheet in **Figure 6**.

Subsequently, the spectral properties of the recorded noise signals were analyzed using the mentioned three microphone pickup patterns. The obtained results are presented for visual comparison in **Figure 7** and summarized in numerical form in **Table 1**; the output statistical parameters of the supplementary spectral features are shown in **Figure 8**.
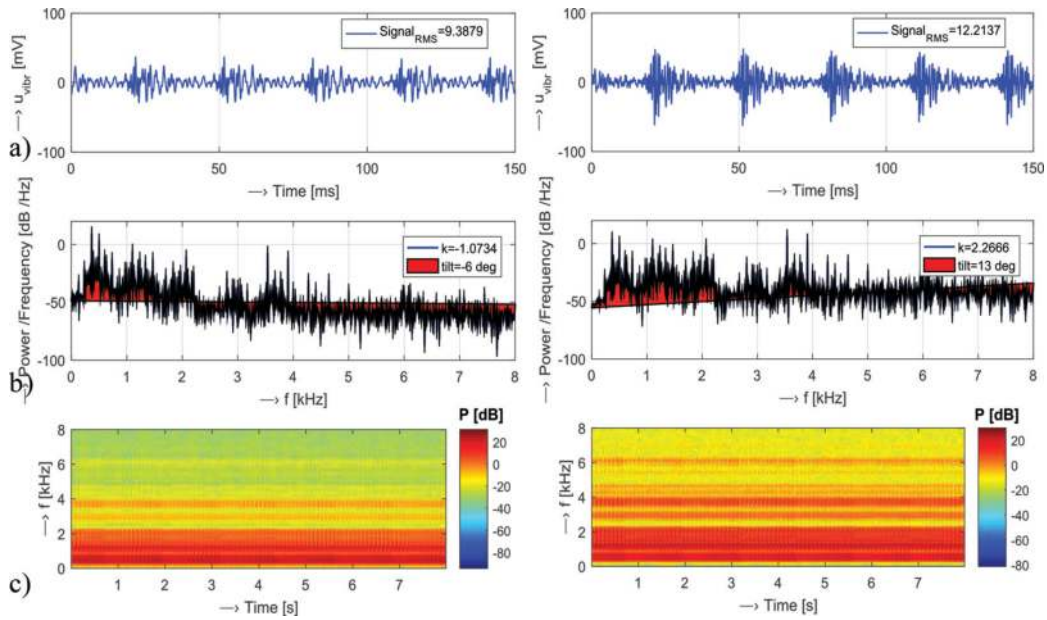
Figure 4.
The vibration signal picked up by the SB-1 sensor without/with the applied shelving filter (left/right set of graphs): selected 150-ms ROI of the signal together with the calculated RMS value (a), corresponding periodogram including the spectral decrease-tilt (b), and spectrogram calculated from the whole 8-s duration of the vibration signal (c); Q = 0.115, f_c = 120, G = 30, and f_s = 16 kHz.
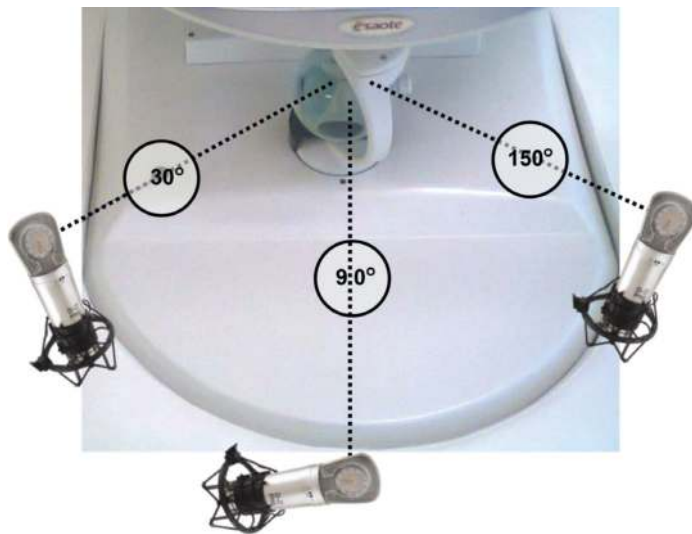

Figure 5.
Principal arrangement of acoustic noise recording in the vicinity of the scanning area of the open-air MRI device Opera: the pickup microphone situated at 30, 90, and 150°.

3.3 Mapping of the acoustic noise SPL in the MRI device vicinity

The acoustic noise SPL was measured using the multifunction environment meter Lafayette DT 8820. In the first step, the dependence of the SPL noise values on the distances D_X was mapped. The measuring device was located successively at the distances of {45, 50, 55, 60, 70, 80, 90} cm from the central point of the scanning area, at the height of 85 cm from the floor (between both gradient coils), and in the direction of 30° from the left corner near the temperature stabilizer, producing majority of the background noise SPL_0—see the experiment
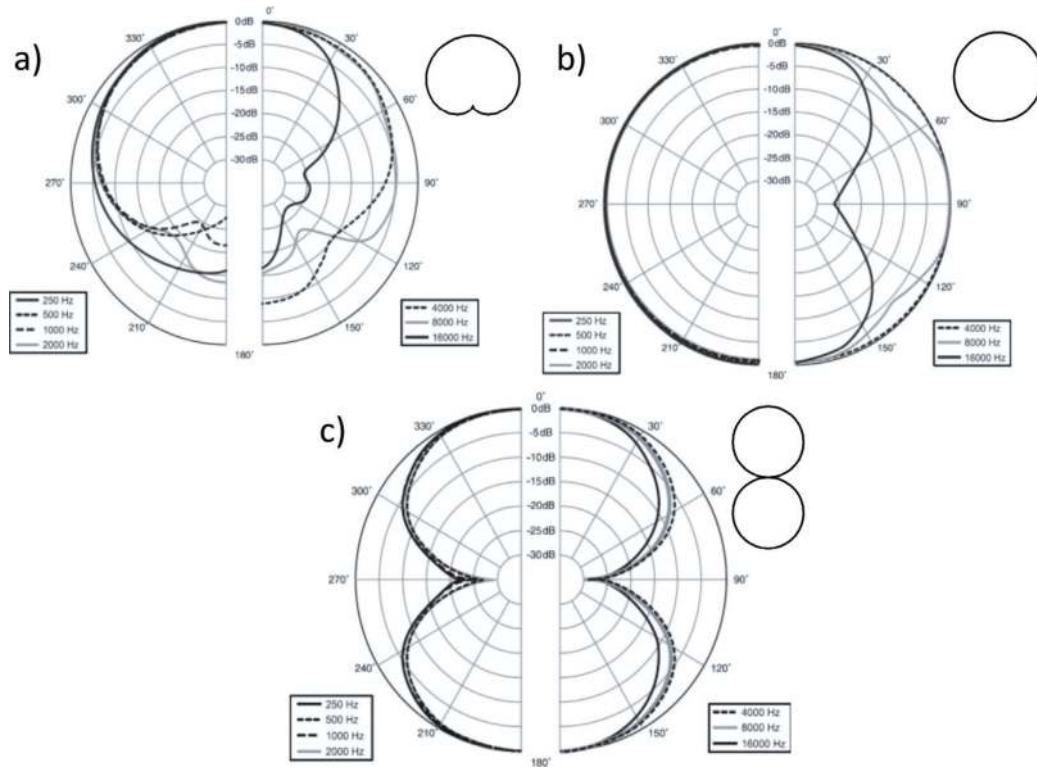
Figure 6.
Example of directional patterns: cardioid (a), omnidirectional (b), and figure-of-eight (c) for the Behringer condenser microphone B-2 PRO.
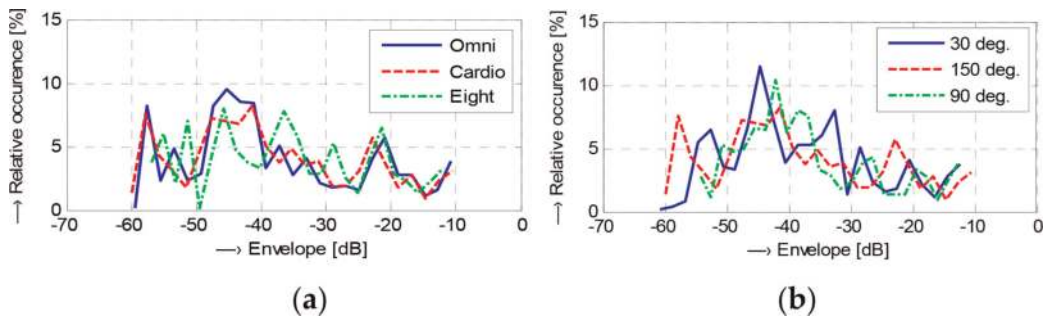

Figure 7.
Comparison of spectral envelope values in [dB] of the noise signals with different directional patterns of the pickup microphone placed at different positions: histograms for omnidirectional, cardioid, and figure-of-eight patterns—signals recorded at 90° (a) and histograms for signals recorded at 30, 90, and 150°—with the cardioid directional pattern (b).

Microphone pickup pattern/ position	At 30°		At 90°		At 150°	
	Signal $_{RMS}$ [−]	S_{tilt} [deg]	Signal $_{RMS}$ [−]	S_{tilt} [deg]	Signal $_{RMS}$ [−]	S_{tilt} [deg]
Omnidirectional	15.3	−16	13.5	−15	14.2	−13
Cardioid	15.2	−11	13.3	−10	14.0	−4
Figure-of-eight	14.1	−18	13.1	−13	13.0	−9

Table 1.
Comparison of the noise spectral parameters of the recordings picked up by the microphone with different directional patterns placed at different positions.
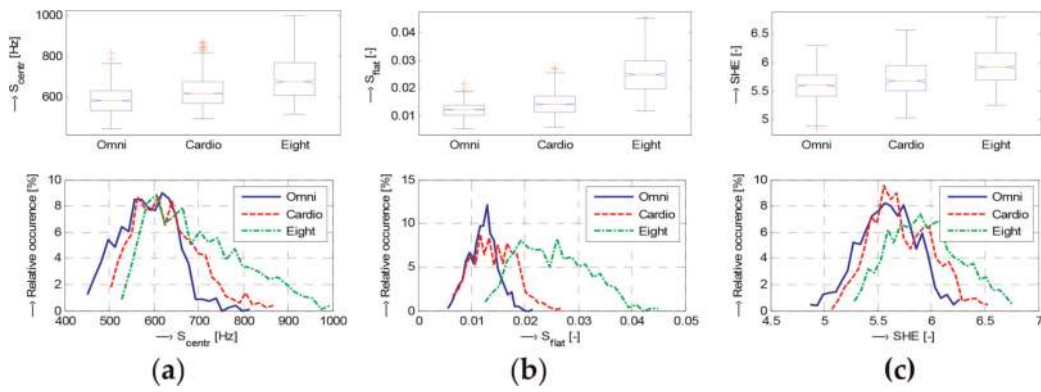
Figure 8.
Supplementary spectral properties of the recorded noise signals with different directional patterns of the pickup microphone—(a) omnidirectional, (b) cardioid, and (c) figure-of-eight; box-plots of the basic statistical parameters in the upper graphs, corresponding histograms of values of the spectral centroid, flatness, and Shannon entropy (in the lower set of graphs); signal recorded at 90°.

arrangement photo in **Figure 9**. Comparison of the resulting SPL values obtained during execution of two basic SE and GE types of the MR scan sequences with the background noise SPL (with no sequence running) is presented in the graphs of **Figure 10**.

3.4 Main measurement experiments with the open-air MRI device

Within the scope of our main experiments, the baseline measurement and recording of the vibration and noise signals were carried out during the execution of the MR scan sequences. For noninvasive testing of the subject/object, usually two basic classes of scan sequences are used to take MR images of human body parts with high quality:
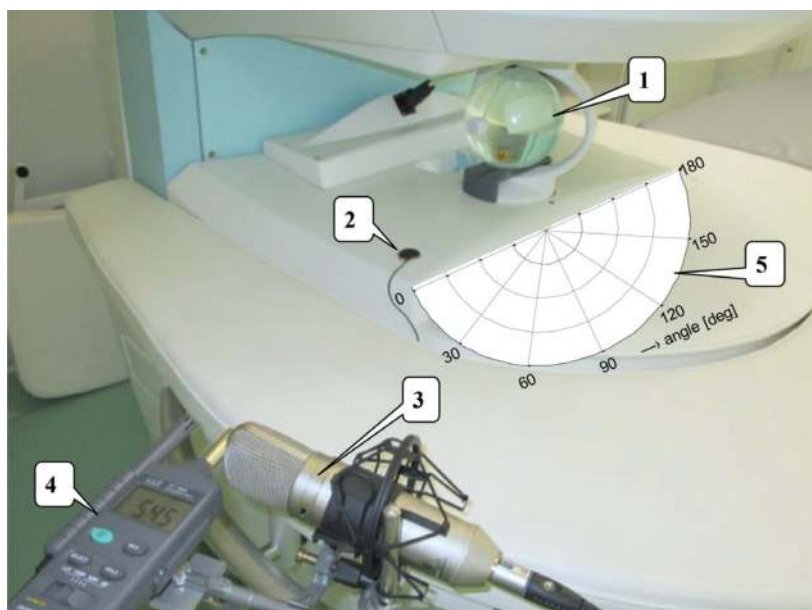

Figure 9.
Arrangement photo of SPL noise measurement and parallel recording of noise and vibration signals of the open-air MRI device Opera: (1) RF knee coil with a spherical water phantom, (2) vibration sensor, (3) pick-up microphone, (4) SPL noise meter, and (5) principal angle diagram of the scanning area.
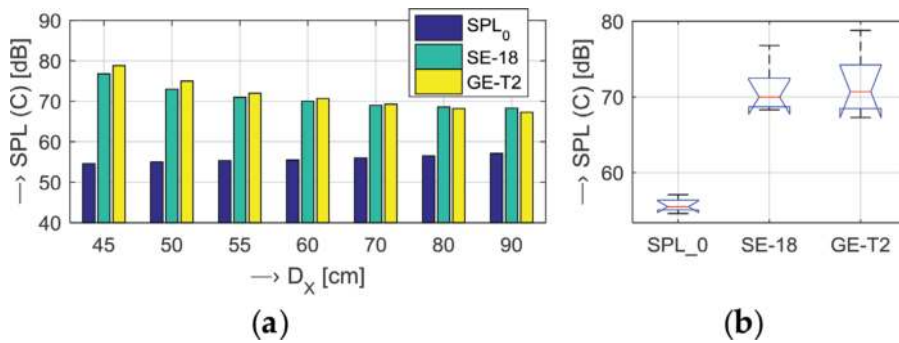
Figure 10.
Mapping of the acoustic noise SPL at different distances D_X = {45, 50, 55, 60, 70, 80, 90} cm from the middle of the scanning area of the MRI device for SE/GE sequences: (a) comparison of the SPL values with those of the background noise (SPL_o) and (b) box-plot of their basic statistical parameters.

- high-resolution (Hi-Res) sequences using the basic SE/GE MRI scan methods [16],

- special 3D sequences used for building or reconstruction of 3D models of biological or botanical issues [17].

Five types of MR scan sequences were tested in total in the investigated MRI device Opera: SE 18 HF, SE 26 HF, GE T2 (as a typical representative of the "Hi-Res" class), SS-3Dbalanced, and 3D-CE [15]. For each of these scan sequences, different settings of the scan parameters are analyzed:

- orientation of scan slices T_{ORIENT} = {Coronal, Sagittal, Transversal}—see visualization of the energy features of the vibration and noise signals in **Figure 11**,
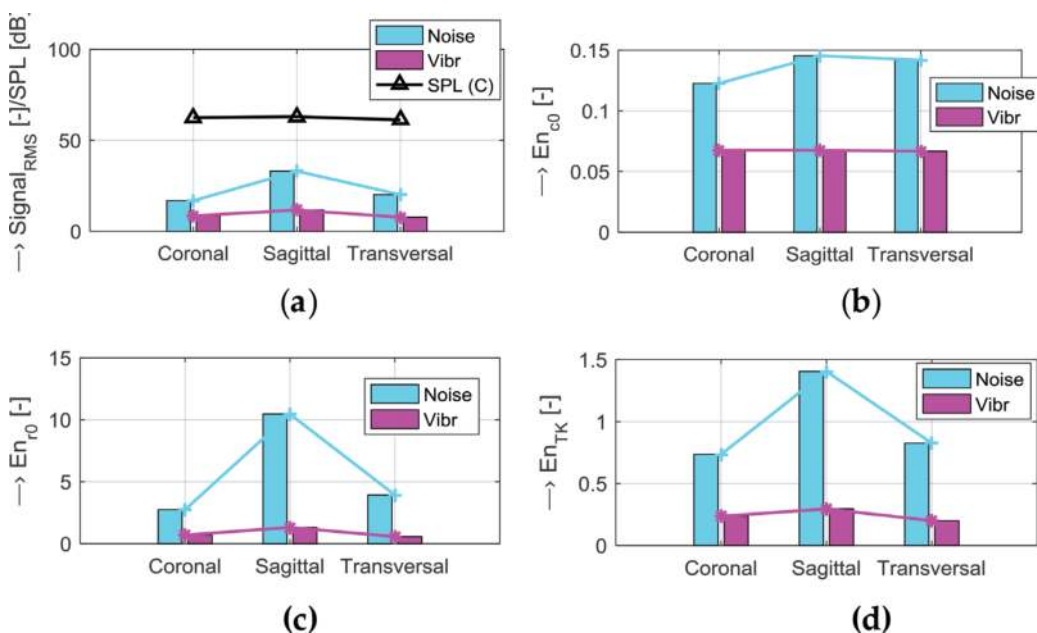

Figure 11.
*Visualization of energy features of the vibration and noise signals for different slice orientations: {coronal, sagittal, transversal}: (a) signal RMS together with noise SPL values, (**b**) mean En_{co}, (c) mean En_{ro}, and (d) mean En_{TK}; used Hi-Res SE scan sequence with TE = 18 ms and TR = 500 ms.*

- echo times T_{TE} = {18, 22, 26} ms—compare the numerical results in **Table 2**,

- repetition time T_{TR} = {60, 100, 200, 300, 400, 500} ms—documented by comparison of the basic statistical parameters calculated from the vibration and noise signals in **Figure 12**,

- mass of the object inserted in the MRI device scanning area {testing phantom/ lying person}—see graphical comparison of the mean values of the energy and basic spectral properties of the vibration signal in **Figure 14**.

The slice orientations as well as the TE and TR parameters were set manually to perform measurement and comparison in the range enabled by the current sequence [15]. Practical realization of the last part of the experiment consists in placing a testing phantom or a head and a neck of a lying person in the RF scan coil between the upper and lower gradient coils of the MRI device. While the total weight of the used testing phantom in the first part of the experiment was 0.75 kg, the weighs of one male and one female voluntary person lying on the patient bed of the MRI device were approx. 80 and 55 kg.

The multisignal measurement comprised real-time recording of the vibration signal by the piezoelectric sensor located inside the scanning area of the investigated

Sequence[1]	Vibrations (SB-1)				Noise[2] SPL (C) [dB]
	Signal $_{RMS}$[−]	En_{TK} [−]	En_{co}[−]	En_{ro}[−]	
TE = 18 ms	31.5 (1.53)	4.32 (0.67)	0.044 (0.002)	23.04 (4.7)	61.5
TE = 22 ms	34.6 (2.11)	4.96 (1.02)	0.040 (0.003)	24.03 (8.5)	62.5
TE = 26 ms	36.0 (2.27)	5.75 (0.85)	0.055 (0.004)	24.40 (9.3)	63.0

[1]Used Hi-Res SE-HF scan sequences with TR = 500 ms and sagittal orientation.
[2]Measured at the distance of D_X = 60 cm and the angle of 30°, SPL_0 = 56 dB.

Table 2.
Comparison of the mean energetic parameters of the vibration signal and the acoustic noise SPL (together with std. values in parentheses) for different settings of the TE time.
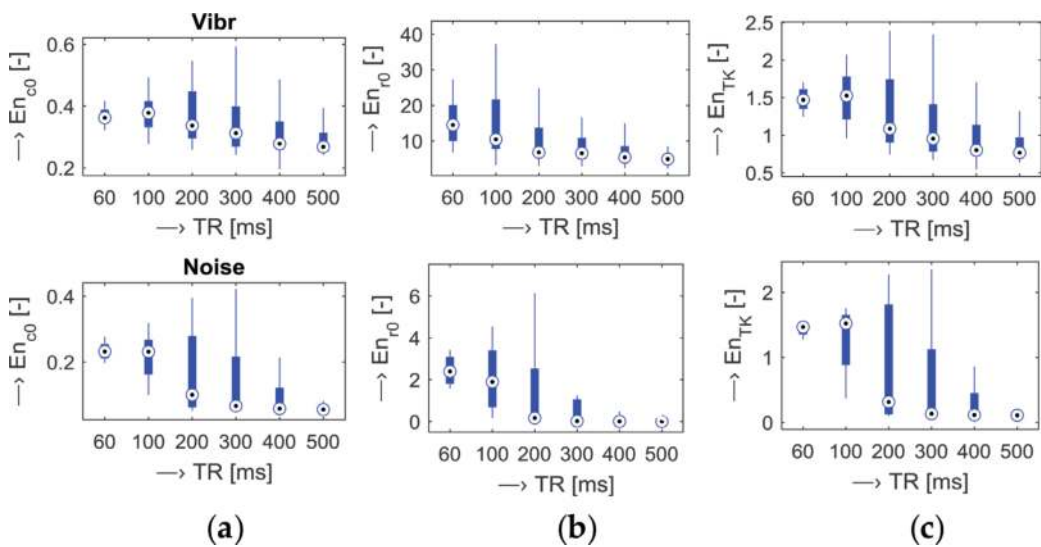

Figure 12.
Visualization of energetic relations of the vibration (upper set of graphs) and noise (lower set) signals for different TR times; {60, 100, 200, 300, 400, 500} ms—basic statistical parameters of: (a) En_{co}, (b) En_{ro}, and (c) En_{TK}; used Hi-Res GE-T2 sequences with TE = 22 ms and sagittal orientation.

MRI device and of the acoustic noise signal using the microphone in its proximity, and the additional measurement to check the noise SPL. In this part of the measurement, the microphone stand with the Behringer dual-diaphragm condenser microphone B-2 PRO was placed together with the SPL meter at the distance of D_X = 60 cm, and the 140-mm diameter spherical testing phantom filled with doped water [15] was placed inside the knee RF coil. The SB-1 sensor [12, 18] was used to pick up the vibration signal inside the scanning area of the MRI Opera device. Practical position of the sensing disc was on the surface of the plastic holder of the bottom gradient coils, as can be seen in the arrangement photo in **Figure 9**. The stored recordings were further processed in order to evaluate and compare the measured signal properties. All the noise and vibration signals were recorded with the help of the Behringer Podcast Studio equipment. The signals with duration of about 15 s sampled at 32 kHz were next processed in the sound editor program Sound Forge 9.0a.

3.5 Analysis of the influence of the scan parameters on the time duration and the quality factor of the MR images

The chosen type of the scanning sequence and the values of the resulting basic scan parameters (TR and TE) have significant influence on the scanning time. These parameters can also be changed manually, but their final values depend on the setting of the other scan parameters—number of slices, slice thickness, number of used accumulations N_{ACC} of the free induction decay (FID) signal [8, 16], etc. Practical demonstration of the acquired MR images with increasing quality factor (Q_F) shows greater range of visible details in the images for three different MR scans of the human vocal tract in **Figure 15**.

The console program "ESAMRI" of the MRI device control software [15] was used to carry out the following two parts of the analysis and comparison:

1. Influence of the basic setting of scan parameters on the final quality factor of MR images and on the time duration T_{DUR} of the scan sequence execution for:

   - different slice thickness of {2, 2.5, 3, 4, 4.5, 5, 10} mm—the predicted Q_F values are presented in **Table 3** for the scan sequence Hi-Res SE18 HE,

   - different repetition times of {60, 100, 200, 300, 400, 500} ms together with N_{ACC}—see visualization of the graphical results using the "Hi-Res" sequences of SE and GE types in **Figure 16**, and T_{DUR} values in **Table 4** for both Hi-Res sequences types,

   - increased number of applied accumulations of the FID signal: N_{ACC} = {1, 2, 3, 4, 5, 6, 7, 8, 10, 16}—the predicted values of Q_F and T_{DUR} are shown numerically in **Table 5** for the scan sequence Hi-Res SE18 HE.

Parameters[1]	Slice thickness [mm]						
	2	2.5	3	4	4.5	5	10
Q_F [−]	17	21	26	34	38	43	85

[1]T_{DUR} = 1 min 39 sec in all cases.

Table 3.
Influence of the slice thickness on the predicted quality factor of the MR image and on the time duration for the scan sequence Hi-Res SE18 HE (TR = 500 ms, N_{ACC} = 1).

N_{ACC} [−]	TR [ms]					
	60	**100**	**200**	**300**	**400**	**500**
1	0:14	0:22	0:41	1:09	1:20	1:39
8	1:35	2:37	5:12	7:46	10:20	12:55
16	3:08	5:11	10:20	15:29	20:38	25:47

Table 4.
Dependence of the time duration T_{DUR} *[min:sec] on setting of TR and* N_{ACC} *parameters—merged values for both Hi-Res sequences of SE and GE types; slice thickness = 4.5 mm.*

Parameters	N_{ACC} [−]									
	1	**2**	**3**	**4**	**5**	**6**	**7**	**8**	**10**	**16**
Q_F [−]	14	20	24	28	31	34	37	40	44	56
T_{DUR} [min:sec]	0:14	0:26	0:37	0:49	1:00	1:12	1:24	1:35	1:58	3:08

Table 5.
Influence of the number of FID signal accumulations on the predicted quality factor of the MR image and on the time duration for the scan sequence Hi-Res SE18 HE (TR = 60 ms and slice thickness = 10 mm).

Parameters	N_{ACC} [−]					
	1	**2**	**3**	**4**	**8**	**16**
Q_F [−]	59 (102)	84 (144)	103	118 (204)	167	237
T_{DUR} [min:sec]	3:14 (5:36)	6:25 (11:04)	9:37	12:48 (22:00)	25:34	51:05

Table 6.
Influence of the number of FID signal accumulations on the predicted quality factor of the MR image and on the time duration for the scan sequence SS-3D balanced (TE = 10 ms and TR = 20 ms) and 3D phases = 24 (for 42 phases, the values are in parentheses).

Parameters	N_{ACC} [−]					
	1	**2**	**3**	**4**	**8**	**16**
Q_F [−]	134 (79)	189 (122)	231	267 (137)	378	534
T_{DUR} [min:sec]	1:04 (9:53)	2:00 (19:44)	2:56	3:52 (29:35)	7:36	15:04

Table 7.
Influence of the number of FID signal accumulations on the predicted quality factor of the MR image and on the time duration for the scan sequence 3D-CE (TE = 30 ms and TR = 40 ms) and 3D phases = 8 (for 72 phases the values are in parentheses).

2. Comparison of the predicted Q_F and T_{DUR} values for "3D" types of MR scan sequences—numerical matching of the results for the changed number of FID signal accumulations and different number of 3D phases using:

- the SS-3D-balanced 10 sequences—see the values in **Table 6**,

- the 3D-CE 30 scan sequence (see **Table 7**).

4. Discussion of the obtained results

The performed calibration and frequency response linearization of the piezo-electric vibration sensor enables precise pick-up of vibration signals in the environment of a weak stationary magnetic field and a high-voltage RF signal disturbance that is observed in the scanning area of the MRI device.

Our measurements have shown an inverse relationship between the diameter of the used sensor and the minimum frequency of the vibration picked up from the measured surface. The sensor HM692 with a massive aluminum microphone capsule used in phonocardiography had the lowest sensitivity and caused the greatest decrease of the maximum frequency. The calibration of the SB2 sensor was carried out in parallel for both pickup elements. The measured frequency responses *SB2a,b* are practically identical with nonlinear decrease in the range of low frequencies from 35 to 100 Hz—see the frequency responses in **Figure 3a**. In 3D scanning of the human vocal tract [4, 5, 19], the MRI device generates the acoustic noise of frequencies in the range from 25 Hz to 3.5 kHz that is similar to the basic frequency range of speech signals. For this reason, the SB-1 sensor was chosen for its greatest size allowing the best low-frequency sensitivity.

Comparison of noise spectral properties recorded for different types of directional patterns of the pickup microphone yields the best recording conditions for the cardioid pattern (minimum spectral decrease as shown by the obtained results in **Table 1**). On the other hand, dispersion of the spectral envelope values is similar for all three analyzed pattern types as can be seen in histograms in **Figure 7a**. Comparison of different microphone positions has shown that at 30°, the background noise from the MRI temperature stabilizer degrades the recording (see the signal RMS values in **Table 1**) and the direction of 150° is a bit unnatural from the point of view of an examined person lying in the MRI scanning area. Therefore, the direction chosen as the best for noise and speech signal recording was in the main horizontal axis of the MRI device (at 90°). In addition, at this position, the lowest values of the noise signal RMS were measured and the smallest dispersion of the spectral envelopes was observed—see the green dash-dot line in **Figure 7b**.

The results of a detailed measurement of the acoustic noise intensity at different distances from the central point of the scanning area for the SE and GE "Hi-Res" sequences are presented in **Figure 10**. The GE sequence produces noise with a slightly higher intensity, then the SE one (approx. 3-dB difference in the nearest location of 45 cm from the center of the scanning area) and variation of the SPL values depending on the measuring distance is also greater as seen in the box-plot graph in **Figure 10b**. The minimum distance was set to 45 cm in order to eliminate interaction of metal parts of the SPL meter with the static magnetic field of the MRI device. If the SPL meter was placed near the center, the field homogeneity would be disrupted and the warning message on the MRI control console would be followed by disabling to run any scan sequence by the software system [14]. The maximum measuring distance was set to 90 cm where the measured MRI noise was masked by the background noise originating from the temperature stabilizer. In the middle of the investigated measuring distances, the SPL values were similar for both types of MR scan sequences, so the working distance of 60 cm was used for all further measurements.

Next investigation of the recorded vibration and noise signals was aimed at the influence of the choice of the slice orientation on the energy of the produced vibration and noise signals. This effect is large—the maximum can be found in the sagittal plane and the minimum in the transversal plane for the vibration signals,

and in the coronal plane for the noise signals—see the column charts in **Figure 11**. Therefore, the remaining experiments used only the sagittal orientation.

In accordance with our previous research [12, 18] the current experiments confirm the influence of the TE and TR times on the vibration and acoustic noise properties. The TE time extension causes fall of the final signal energy as documented by raised all the four determined vibration energetic parameters as well as the achieved SPL noise values in **Table 2**. The influence of the TR time determining the basic dominant frequency can be seen in box-plot graphs in **Figure 12**. This visualization of the basic statistical parameters obtained from analysis of vibration and noise signals shows the highest values of all energetic parameters for the shortest TR times (60 or 100 ms).

Comparison of energetic relations of the vibration and noise signals for different sequence types brings ambiguous results and shows only small differences—see three bar-graphs in **Figure 13**. The 3D sequence "SS-3Dbalanced" differs from the remaining sequence types by reverse behavior: while the En_{c0} and En_{r0} parameters indicate the minimum values, the En_{TK} achieves the maximum ones (see the graph in **Figure 13c**). This situation can be caused by the minimum settings of the TE and TR times that were used for the "Hi-Res" types to be comparable with the "3D" types with slightly atypical values being out of the normal range of use although the control software enables their setting [15].

Next comparison of energetic relations of the vibration and noise signals for different objects placed in the scanning area of the MRI device shows a relatively high effect of the mass put upon the bottom plastic holder of the gradient coils. The effective weight of the person exerting a pressure on the bottom plastic holder of the gradient coils attenuates the vibration pulses partially. The mass effect is demonstrated by increase of the vibration signal energy based on En_{c0} parameter with its maximum for the lying male person with the weight of 80 kg (see the bar-graph in **Figure 14a**). It is also demonstrated in the spectral properties of the vibration
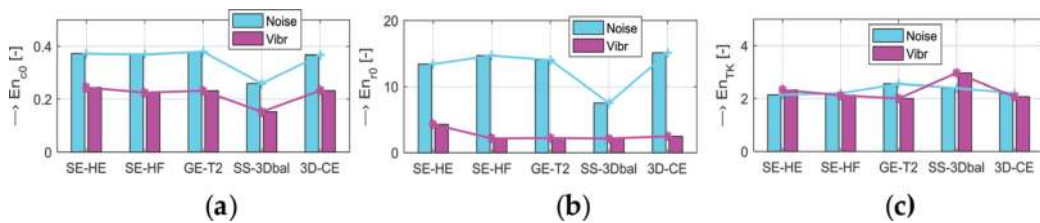

Figure 13.
Comparison of energetic relations of vibration and noise signals for different sequence types: {Hi-Res SE-HE, Hi-Res SE-HF, Hi-Res GE-T2, SS-3Dbal, 3D-CE}: (a) mean En_{co}, (b) mean En_{ro}, and (c) mean En_{TK}; in all cases, the sagittal slice orientation was used.
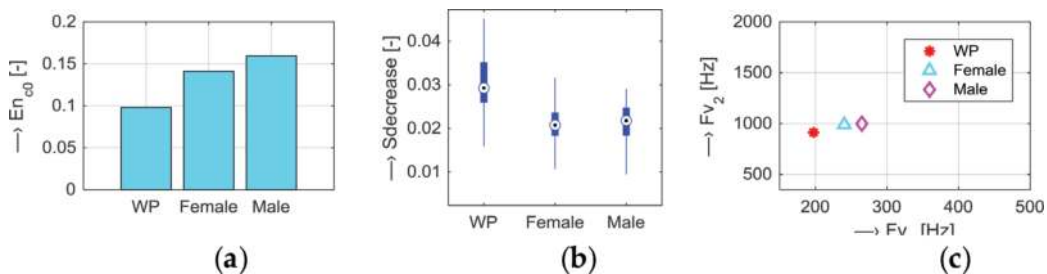

Figure 14.
Comparison of mean values of the energy and basic spectral properties of the vibration signal for different objects placed in the scanning area of the MRI device: (a) energy En_{co}, (b) box-plot of basic statistical properties for the spectral decrease values, and (c) mutual values of the frequencies F_{V1} and F_{V2}; used Hi-Res SE-HF scan sequences with TE = 18 ms, TR = 400 ms, and sagittal orientation.
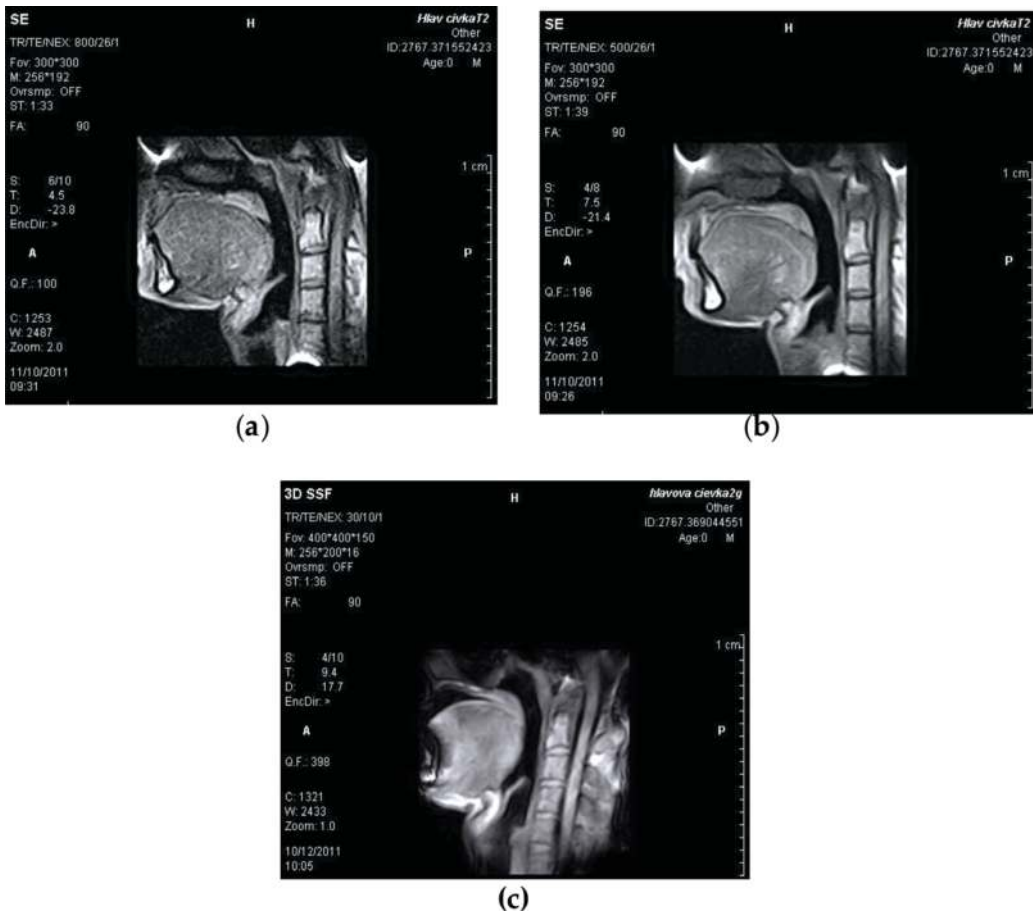
Figure 15.
Examples of MR images of the human vocal tract obtained with different values of the quality factor: (a) scan sequence Hi-Res SE26 HF (TR = 500), slice thickness = 4.5 mm, Q_F = 100, (b) scan sequence Hi-Res SE26 HF (TR = 500), slice thickness = 7.5 mm, Q_F = 196, and (c) scan sequence 3D SSF 30 (TR = 10), slice thickness = 9.4 mm, and Q_F = 398.
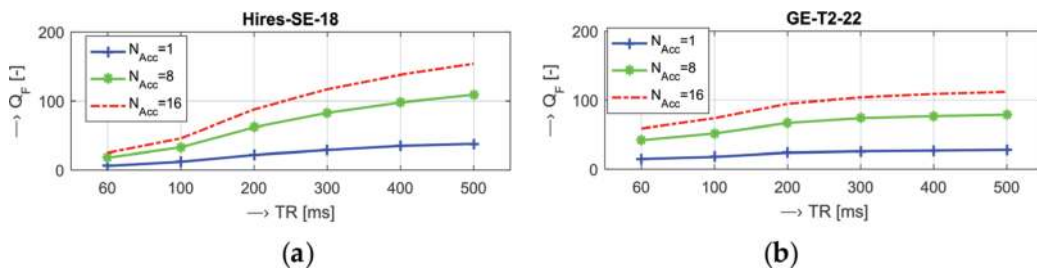

Figure 16.
Influence of the TR time and the number of FID signal accumulations on the predicted image quality factor for the Hi-Res sequences of—(a) SE and (b) GE type; slice thickness = 4.5 mm.

signal as shown by lower spectral decrease in **Figure 14a** and by shift of the first two dominant frequencies toward higher values—see the mutual $F_{V1,2}$ position in **Figure 14c**.

Results of the preliminary analysis of influence of the slice thickness document that its increase has a positive effect on the predicted quality factor of MR images—compare the values in **Table 3**. Next comparison shows a positive influence of increase in the TR time on the quality factor, and this effect is more pronounced when using the SE sequence type—see the left graph in **Figure 16**. This figure also documents significant dependence between the applied number of FID signal

accumulations and the predicted Q_F value. Also, in this case, the increase of Q_F is more distinctive for the SE sequences. Values in **Table 4** describe the influence of TR and N_{ACC} values on the final time duration of the executed scan sequence. While the increased TR causes only moderately greater overall time duration, the changed N_{ACC} parameter has comparably higher influence on the final time duration. This effect is also shown in a detailed comparison of numerical results for different N_{ACC} values in **Table 5**. For the "Hi-Res" sequence types, the increase of the parameter N_{ACC} from 2 to 16 results in about 2.8 times greater value of Q_F but 6 times greater than that of T_{DUR}. For the "3D" sequence types, the increase of the resulting time duration is also affected by the choice of the number of 3D phases (equivalent to the number of slices with selection of the slice thickness for the "Hi-Res" sequences) in parallel as shown in **Tables 6 and** 7.

5. Conclusions

Acoustic noise measurement in the vicinity of the investigated open-air MRI device yielded the maximum sound pressure level of about 82 dB(C) at the distance of 45 cm from the central point of the MRI scanning area for the GE scan sequence with short TE and TR times and the sagittal orientation of scan slices. For examination of other parts of the human body (leg, arm, etc.), the head is not inserted directly between the upper and the lower gradient coils, so the noise level is much lower as documented for different distances in **Figure 10**. Finally, the scanning times for the mostly used 3D or Hi-Res sequences are in general less than 15 minutes (typically about 3–5 minutes depending on the chosen number and thickness of the slices)—exposition of the examined person and his/her hearing system to the noise and vibration is not significant.

If there is need for more detailed MR images with higher quality factor Q_F (e.g., in scanning of particular parts of the human brain, the eye, the middle and inner ear, etc.), the time duration T_{DUR} can be much longer (more than half an hour). In such a case, the long exposition to the vibration and acoustic noise may impose great physiological and psychological stress on the patient. Therefore, these scan parameters should be chosen only in the urgent cases.

The results of the performed measurements are useful for precise description of the process of the mechanical vibration excitation and the acoustic noise radiation in the scanning area and in the vicinity of the MRI device. The measurement results and comparisons with a similar low-field MRI tomograph can be used in optimization of the acoustic noise suppression in the speech recorded parallel with application of MRI scanning for 3D modeling of the human vocal tract [19].

Acknowledgements

Conflict of interest

The authors declare no conflict of interest.

Author details

Jiří Přibil[1]*, Anna Přibilová[2] and Ivan Frollo[1]

1 Institute of Measurement Science, SAS, Bratislava, Slovak Republic

2 Institute of Electronics and Photonics, Faculty of Electrical Engineering and
Information Technology, SUT, Bratislava, Slovak Republic

*Address all correspondence to: umerprib@savba.sk

IntechOpen

References

[1] He Z, He W, Wu J, Xu Z. The novel design of a single-sided MRI probe for assessing burn depth. Sensors. 2017;**17**: 526. DOI: 10.3390/s17030526

[2] Panych LP, Madore B. The physics of MRI safety. Journal of Magnetic Resonance Imaging. 2018;**47**:28-43. DOI: 10.1002/jmri.25761

[3] Moelker A, Wielopolski PA, Pattynama PMT. Relationship between magnetic field strength and magnetic-resonance-related acoustic noise levels. Magnetic resonance materials in physics. Biology and Medicine. 2003;**16**: 52-55. DOI: 10.1007/s10334-003-0005-9

[4] Mainka A, Platzek I, Mattheus W, Fleischer M, Müller AS. Three-dimensional vocal tract morphology based on multiple magnetic resonance images is highly reproducible during sustained phonation. Journal of Voice. 2017;**31**:504. e11-5504.e20. DOI: 10.1016/j.jvoice.2016.11.009

[5] Kuortti J, Malinen J, Ojalammi A. Post-processing speech recordings during MRI. Biomedical Signal Processing and Control. 2018;**39**:11-22. DOI: 10.1016/j.bspc.2017.07.017

[6] Seidman MD, Standring RT. Noise and quality of life. International Journal of Environmental Research and Public Health. 2010;**7**:3730-3738

[7] Diedrichsen J, Balsters JH, Flavell J, Cussans E, Ramnani N. A probabilistic MR atlas of the human cerebellum. NeuroImage. 2009;**46**:39-46. DOI: 10.1016/j.neuroimage.2009.01.045

[8] Liang ZP, Lauterbur PC. Principles of Magnetic Resonance Imaging: A Signal Processing Perspective. New York: Wiley-IEEE Press; 2000. 416 p. ISBN: 978-0-780-34723-6

[9] Rimell AN, Mansfield NJ, Paddan GS. Design of digital filters for frequency weightings (A and C) required for risk assessments of workers exposed to noise. Industrial Health. 2015;**53**:21-27. DOI: 10.2486/indhealth.2013-0003

[10] Fraden J. Handbook of Modern Sensors: Physics, Designs, and Applications. 4th ed. New York: Springer; 2016. 663 p. ISBN: 978-1-4939-0040-4

[11] Mechefske CK. Vibration in MRI scanners. In: Al-Jumaily A, Alizad A, editors. Biomedical Applications of Vibration and Acoustics in Therapy, Bioeffects and Modeling. New York: ASME Press; 2008. pp. 329-349. ISBN: 978-0-7918-0275-5

[12] Přibil J, Přibilová A, Frollo I. Comparison of mechanical vibration and acoustic noise in the open-air MRI. Applied Acoustics. 2016;**105**:13-23. DOI: 10.1016/j.apacoust.2015.11.013

[13] Zölzer U. Digital Audio Signal Processing. 2nd ed. Chichester: John Wiley & Sons; 2008. ISBN: 978-0-470-99785-7

[14] Boudraa AO, Salzenstein F. Teager–Kaiser energy methods for signal and image analysis: A review. Digital Signal Processing. 2018;**78**:338-375. DOI: 10.1016/j.dsp.2018.03.010

[15] SpA E. E-Scan Opera. Genoa: User's Manual. Revision A; 2008

[16] Bernstein MA, King KF, Zhou XJ. Handbook of MRI Pulse Sequences. Burlington: Elsevier Academic Press; 2004. 1040 p. ISBN: 978-0-12-092861-3

[17] Wellard RM, Ravasio JP, Guesne S, Bell C, Oloyede A, Tevelen G, et al. Simultaneous magnetic resonance imaging and consolidation measurement

of articular cartilage. Sensors. 2014;**14**: 7940-7958. DOI: 10.3390/s140507940

[18] Přibil J, Přibilová A, Frollo I. Mapping and spectral analysis of acoustic vibration in the scanning area of the weak field magnetic resonance imager. Journal of Vibration Acoustic Transaction ASME. 2014;**136**:051005– 01-051005–051010. DOI: 10.1115/ 1.4027791

[19] Přibil J, Přibilová A, Frollo I. Analysis of acoustic noise and its suppression in speech recorded during scanning in the open-air MRI. In: Ahmed N, editor. Advances in Noise Analysis, Mitigation and Control. InTech. Croatia: Rijeka; 2016. pp. 205-228